



Reduced [¹⁸F]flortaucipir retention in white matter hyperintensities compared to normal-appearing white matter

Alexis Moscoso^{1,2} · Michel J. Grothe^{1,2,3,4} · Michael Schöll^{1,2,5} · for the Alzheimer's Disease Neuroimaging Initiative

Received: 20 September 2020 / Accepted: 4 January 2021

© The Author(s), under exclusive licence to Springer-Verlag GmbH, DE part of Springer Nature 2021

Abstract

Purpose Recent research has suggested the use of white matter (WM) reference regions for longitudinal tau-PET imaging. However, tau tracers display affinity for the β -sheet structure formed by myelin, and thus WM lesions might influence tracer retention. Here, we explored whether the tau-sensitive tracer [¹⁸F]flortaucipir shows reduced retention in WM hyperintensities (WMH) and how this retention changes over time.

Methods We included 707 participants from the Alzheimer's Disease Neuroimaging Initiative with available [¹⁸F]flortaucipir-PET and structural and FLAIR MRI scans. WM segments and WMH were automatically delineated in the structural MRI and FLAIR scans, respectively. [¹⁸F]flortaucipir standardized uptake value ratios (SUVR) of WMH and normal-appearing WM (NAWM) were calculated using the inferior cerebellar grey matter as reference region, and a 3-mm erosion was applied to the combined NAWM and WMH masks to avoid partial volume effects. Longitudinal [¹⁸F]flortaucipir SUVR changes in NAWM and WMH were estimated using linear mixed models. The percent variance of WM-referenced cortical [¹⁸F]flortaucipir SUVRs explained by longitudinal changes in the WM reference region was estimated with the R^2 coefficient.

Results Compared to NAWM, WMH areas displayed significantly reduced [¹⁸F]flortaucipir SUVR, independent of cognitive impairment or A β status (mean difference = 0.14 SUVR, $p < 0.001$). Older age was associated with lower [¹⁸F]flortaucipir SUVR in both NAWM (-0.002 SUVR/year, $p = 0.005$) and WMH (-0.004 SUVR/year, $p < 0.001$). Longitudinally, [¹⁸F]flortaucipir SUVR decreased in NAWM (-0.008 SUVR/year, $p = 0.03$) and even more so in WMH (-0.02 SUVR/year, $p < 0.001$). Between 17% and 66% of the variance of longitudinal changes in cortical WM-referenced [¹⁸F]flortaucipir SUVRs were explained by longitudinal changes in the reference region.

Data used in preparation of this article were obtained from the Alzheimer's Disease Neuroimaging Initiative (ADNI) database (adni.loni.usc.edu). As such, the investigators within the ADNI contributed to the design and implementation of ADNI and/or provided data but did not participate in the analysis or the writing of this report. A complete listing of ADNI investigators can be found at: http://adni.loni.usc.edu/wpcontent/uploads/how_to_apply/ADNI_Acknowledgement_List.pdf

This article is part of the Topical Collection on Neurology – Dementia

✉ Michel J. Grothe
mgrothe@us.es

✉ Michael Schöll
michael.scholl@neuro.gu.se

¹ Department of Psychiatry and Neurochemistry, Institute of Neuroscience and Physiology, The Sahlgrenska Academy, University of Gothenburg, Gothenburg, Sweden

² Wallenberg Centre for Molecular and Translational Medicine, University of Gothenburg, Gothenburg, Sweden

³ Unidad de Trastornos del Movimiento, Instituto de Biomedicina de Sevilla (IBiS), Hospital Universitario Virgen del Rocío/CSIC/ Universidad de Sevilla, Avda. Manuel Siurot, s/n, 41013 Sevilla, Spain

⁴ Grupo Trastornos del Movimiento, Instituto de Biomedicina de Sevilla, Campus Hospital Universitario Virgen del Rocío, Avda. Manuel Siurot, s/n, 41013 Sevilla, Spain

⁵ Department of Neurodegenerative Disease, UCL Queen Square Institute of Neurology, University College London, London, UK

Conclusions [^{18}F]flortaucipir retention in the WM decreases over time and is influenced by the presence of WMH, supporting the hypothesis that [^{18}F]flortaucipir retention in the WM is partially myelin-dependent. These findings have implications for the use of WM reference regions for [^{18}F]flortaucipir-PET imaging.

Keywords Tau PET · White matter · Hyperintensity · Reference region · Myelin · Longitudinal

Introduction

The advent of positron emission tomography (PET) imaging with tau-sensitive tracers has enabled the *in vivo* detection and quantification of tau neurofibrillary tangle (NFT) pathology [1–3], a pathological hallmark of Alzheimer’s disease (AD) [4]. Consistent with prior neuropathological studies [5], PET-measured NFT burden has been consistently found to be closely related to neurodegeneration and cognitive decline among individuals on the AD continuum [6–12]. Motivated by these results and the failure of several anti-amyloid- β ($\text{A}\beta$) drugs [13], tau has therefore been proposed as a promising therapeutic target in AD [14]. Moreover, recent studies have reported that serial tau PET imaging with [^{18}F]flortaucipir (FTP) could be used to track changes in NFT burden [15–17], suggesting that longitudinal FTP PET might be useful for assessing the effectiveness of both $\text{A}\beta$ - and tau-targeting treatments [18].

Despite significant progress in the field, several aspects of the quantification of longitudinal change in NFT burden using FTP PET remain to be investigated. Chief among them is the choice of reference region for deriving longitudinal standardized uptake value ratios (SUVR). The use of white matter (WM) reference regions has become popular among several research groups [6, 16, 19] given their improved stability and discriminative properties compared to traditional cerebellar reference regions [20]. However, FTP retention in the WM is poorly understood, and no prior studies have systematically investigated how WM abnormalities associated with advanced age or how potentially existing pathology might influence FTP retention in the WM. Therefore, and stability issues aside, it is unclear whether the use of WM reference regions is actually beneficial for a more accurate quantification of the cortical FTP PET signal of interest.

A potential biological process that might influence FTP retention in the WM is myelin loss associated to age-related pathologic processes or even normal aging itself. Similar to $\text{A}\beta$ tracers [21, 22], existing tau tracers base their specificity on the affinity for β -sheet structures adopted by fibrillary forms of the target proteins in AD [23]. This β -sheet structure is, however, also displayed by other proteins such as the myelin basic protein, a major component of axons. Accumulating evidence now indicates that $\text{A}\beta$ tracers show reduced retention in demyelinating WM lesions associated with multiple sclerosis [21, 22, 24–27] as well as in age-related WM

hyperintensities (WMH) [28–30]. Therefore, it is plausible that, similar to $\text{A}\beta$ tracers, FTP binding in the WM could also be influenced by such lesions, potentially confounding longitudinal FTP measures if these regions are used as reference.

Under the premise that FTP binding in the WM may reflect myelin integrity, we hypothesize that (1) WMH regions, which are associated with severe myelin loss [31], would show reduced FTP retention compared to normal-appearing WM (NAWM), and (2) FTP retention in the WM would decrease over time as a consequence of typical age-related myelin loss [32]. Additionally, we explored potential sex-related differences in FTP retention in the WM as menopause has been previously suggested to be associated with a number of WM changes, including myelin loss [33, 34]. To test our hypotheses, we examined multimodal imaging data from more than 700 individuals enrolled in the Alzheimer’s Disease Neuroimaging Initiative who underwent T1-weighted and fluid-attenuated inversion recovery (FLAIR) MRI and FTP PET imaging at multiple time points. As a secondary aim, we quantified the impact of using WM as the reference region in longitudinal measures of cortical FTP PET SUVR.

Methods

Study design

Data used in the preparation of this article were obtained from the Alzheimer’s Disease Neuroimaging Initiative (ADNI) database (<http://adni.loni.usc.edu>). The ADNI was launched in 2003 as a public-private partnership, led by Principal Investigator Michael W. Weiner, MD. The primary goal of ADNI has been to test whether serial MRI, PET, other biological markers, and clinical and neuropsychological assessments can be combined to measure the progression of mild cognitive impairment (MCI) and early AD.

In this study, we included all ADNI3 participants who were either cognitively normal (CN) or cognitively impaired (MCI and AD dementia) and had available FTP PET as well as T1-weighted and FLAIR MRI scans at the same study visit ($n = 707$). The majority of the study participants also underwent $\text{A}\beta$ PET imaging with either [^{18}F]florbetapir or [^{18}F]florbetaben within 2 years from the tau PET visit ($n = 693$) and were categorized as $\text{A}\beta_{\pm}$ on the basis of previously established cut-points [35] (see [!\[\]\(9c2e8d1b5bd77cb5c9f83b7a9cff79fd_img.jpg\) Springer](http://adni.loni.usc.edu/data-</p>
</div>
<div data-bbox=)

[samples/access-data/](#) for [^{18}F]florbetaben cut-point derivation). Longitudinal FTP scans were acquired annually for up to 2.9 years from baseline. One or more longitudinal FTP scans were available in 206 participants over a mean follow-up period of 1.5 years. In this subset, and over the same follow-up period, 197 subjects underwent at least one follow-up MRI scan. Demographic characteristics of study participants are summarized in Table 1.

PET acquisition and pre-processing

FTP PET scans were acquired 75 to 105 min after the injection of 370 ± 37 MBq of FTP, using a dynamic protocol of 6×5 min. [^{18}F]florbetapir and [^{18}F]florbetaben PET scans were acquired 50 to 70 and 90 to 110 min post-injection of 370 ± 37 MBq and 300 ± 30 MBq, respectively. Pre-processing steps for PET scanner harmonization in ADNI were identical for all tracers and have been described previously [36]. In short, individual PET frames were realigned, averaged, reoriented, resliced to a common grid, and smoothed to an isotropic resolution of 8 mm. Further details of PET acquisition protocols and pre-processing steps in ADNI can be found at <http://adni.loni.usc.edu/methods/documents/>.

MRI acquisition and pre-processing

MRI acquisition protocols in ADNI3 are described in detail elsewhere [37] and can be found in <http://adni.loni.usc.edu/methods/documents/mri-protocols/>. All subjects were examined on 3T scanners employing anatomical 3D T1-weighted accelerated MP-RAGE or accelerated SPGR as well as 3D FLAIR sequences. No further pre-processing steps were performed by the ADNI MRI core as MRI scanners in ADNI3

Table 1 Cohort characteristics. Age and [^{18}F]flortaucipir SUVR measures are reported as mean (SD). WMH volume is reported as median (range). CU, cognitively unimpaired; CI, cognitively impaired; MCI, mild cognitive impairment; AD, Alzheimer's disease; A β , amyloid- β ; NAWM, normal-appearing white matter; WMH, white matter hyperintensity; SUVR, standardized uptake value ratio

	CU	CI
Baseline characteristics		
<i>N</i>	404	303
Age, years	73.0 (7.0)	75.2 (8.1)
Sex, M/F	162/242	172/131
MCI/AD		226/77
A β -positive, <i>n</i> (%)	134 (34) (missing = 5)	168 (57) (missing = 9)
NAWM SUVR	1.14 (0.12)	1.17 (0.14)
WMH SUVR	1.01 (0.14)	1.01 (0.14)
WMH volume (cm ³)	1.9 (0.0 to 52.5)	4.0 (0.0 to 139.3)

perform online gradient unwarping and intensity normalization as part of the image reconstruction pipeline.

Image analysis

WM and WMH segmentation

Structural T1-weighted MRI scans were segmented into grey matter (GM) and WM tissue probability maps and spatially registered to MNI standard space using Statistical Parametric Mapping 12 (SPM12; Wellcome Department of Imaging Neuroscience, Institute of Neurology, London, UK). Individual WM masks were obtained by thresholding the corresponding probability map at > 0.5 . The inverse of the deformation field from spatial registration was then used to propagate a cerebral mask from MNI space into each individual's native space, and this mask was intersected with the previously derived WM mask to obtain a cerebral WM mask (i.e., excluding the brainstem and cerebellar WM).

WMH masks were derived using the Lesion Growing Algorithm [38] implemented in the Lesion Segmentation Toolbox (LST, SPM12) (<https://www.applied-statistics.de/lst.html>). Briefly, this pipeline combines information from the T1-derived tissue probability maps and the FLAIR images to create lesion belief maps that are iteratively grown by adding voxels that appear hyperintense, resulting in individual WMH probability maps in T1 space. The algorithm needs a tuning parameter (κ) to be specified, which was set to 0.25 as in previous studies using ADNI data [39, 40]. Binary WMH masks were created by retaining only voxels with probability = 1 in the lesion probability map [38]. Finally, we intersected the previous cerebral mask with the WMH mask to retain only cerebral WMH.

FTP PET analysis

To quantify FTP retention in cerebral WM, we performed the following steps: First, FTP scans (both baseline and, if available, follow-up) were coregistered to the corresponding baseline T1 MRI scan using SPM12. Second, we created standardized uptake value ratio (SUVR) images by dividing each voxel intensity by the mean signal in the inferior portion of the cerebellar grey matter [41]. For this, the reference signal was measured in the intersection between an individual's GM mask (thresholded at 0.5) and the inferior portion of the SUIT cerebellar atlas propagated to T1 MRI native space [42]. Third, we excluded small WMH clusters with fewer than 27 voxels (~ 27 mm³, corresponding to a 3-mm isotropic voxel) from the analysis to avoid excessive contamination due to possible spill-in counts from surrounding NAWM [25]. Fourth, to avoid partial volume effects (PVE), we performed a 3-mm erosion in the combined WM and WMH mask so that all the voxels at distance ≤ 3 mm from any non-WM

structure were excluded. Furthermore, we also excluded thalamic WM given its known off-target binding properties in FTP PET [42]. Finally, we computed average SUVRs within this eroded cerebral WM mask in both WMH and NAWM (we define NAWM as the voxels in the eroded cerebral WM mask not labeled as WMH). In order to confirm that our findings were not driven by PVE, we recalculated the above-described measures using two-compartment PVE correction [43] and reran all associated analyses (see Supplementary Methods). Moreover, we measured longitudinal FTP SUVR in cerebellar WM, a region in which we did not observe WMH, to further investigate whether our longitudinal findings in NAWM were driven by the presence or the longitudinal progression of adjacent WMH.

To perform voxelwise FTP analyses in the WM, we spatially normalized the FTP SUVR images using the deformation field derived from spatial registration of the T1 MRI scan, applied an isotropic 6-mm smoothing filter, and masked the final image using a WM mask of the MNI space template. Although no erosion was performed on these data, we repeated these analyses using PVE correction to further confirm that the associations were not driven by PVE (see Supplementary Methods and Supplementary Figures 2 and 4).

To study the impact of WM FTP retention changes on longitudinal cortical FTP SUVRs based on WM reference regions, we computed baseline and follow-up FTP SUVRs in a predefined AD-specific cortical composite Meta-ROI [44] comprising entorhinal, amygdala, parahippocampal, fusiform, inferior temporal, and middle temporal cortical ROIs, using (1) an eroded hemispheric WM ROI as defined in ADNI as reference region [45] and (2) a data-driven WM reference region as defined by the PERSI method [20].

Statistical analysis

We assessed NAWM SUVR vs WMH SUVR differences using paired *t* tests and reporting mean difference with 95% confidence intervals. Associations between WM FTP SUVR

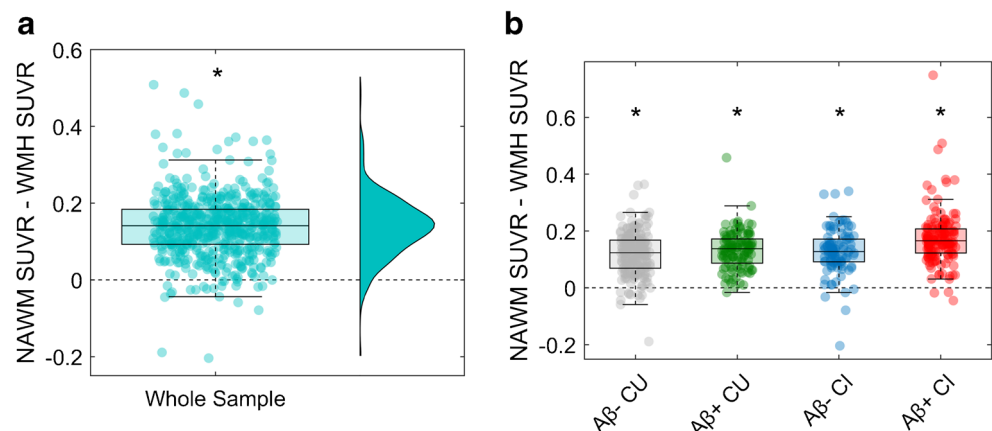
and age were tested both at the voxel and ROI levels (NAWM and WMH) using linear correlation analysis (Pearson's *r*). To understand whether total WMH volume influences the previous associations, we reran these analyses adjusting for total WMH volume. Furthermore, we explored potential sex differences in FTP SUVR in the WM using age-adjusted linear regressions. In longitudinal analyses, we assessed WM FTP SUVR changes over time as well as time×sex and time×WMH annual change interactions using linear mixed models with subject-specific intercepts and slopes, both at the voxel level and in NAWM and WMH ROIs. Rates of annual change were computed using linear regressions. Associations between the annual rates of change of cortical Meta-ROI FTP SUVRs (using eroded WM as the reference region) and eroded WM FTP SUVRs (using the inferior cerebellar grey matter as the reference region) were estimated using linear regressions, and we computed the amount of variance of cortical Meta-ROI FTP SUVR change attributable to changes in the eroded WM region as the R^2 coefficient between these two measures. Results from cross-sectional voxelwise analyses were assessed using a cluster-level significance threshold of $p_{FWE} < 0.001$, with an initial voxelwise height threshold of $p_{FDR} < 0.001$. In order to maintain a similar statistical power in the longitudinal analysis of the smaller subset of participants, the initial voxelwise height threshold was set to $p_{FDR} < 0.05$ for this analysis, with the same cluster-level significance threshold of $p_{FWE} < 0.001$ [46].

Results

Reduced FTP retention in WMH compared to NAWM

After the erosion procedure, 561 subjects demonstrated at least some areas of WMH. Compared to NAWM, WMH areas showed significantly reduced FTP SUVR (mean difference = 0.14, [0.13 to 0.15], Fig. 1A). This difference was still present when participants were stratified according to A β status and

Fig. 1 Subject-specific difference between NAWM and WMH [18 F]flortaucipir SUVR for (A) the whole sample and (B) subjects stratified by A β pathology and cognitive impairment. NAWM, normal-appearing white matter (eroded); WMH, white matter hyperintensity (eroded); SUVR, standardized uptake value ratio; A β , amyloid β . * $p < 0.001$



cognitive impairment (CU and CI) (Fig. 1B), with mean differences varying from 0.12 (0.11 to 0.13) SUVR in A β - CU to 0.17 (0.16 to 0.18) SUVR in A β + CI, as well as after performing PVE correction (Supplementary Figure 1). Illustrative examples of four study participants with high WMH burden displaying reduced FTP retention in these regions are depicted in Fig. 2.

Reduced FTP retention in the WM with advancing age

Voxelwise analyses on cross-sectional data demonstrated that FTP retention in the WM decreases with advancing age (Fig. 3A). The spatial association pattern involved extensive areas of bilateral deep and periventricular WM, as well as the corpus callosum. These associations were still observed after PVE correction (Supplementary Figure 2A) and after adjusting for total WMH volume (Supplementary Figure 3). In cross-sectional ROI analyses, FTP SUVRs in both NAWM and WMH decreased with increasing age (Fig. 3B). PVE correction yielded consistent results, although the association for NAWM was found to be on a statistical trend level ($b = -0.0012$ SUVR/y, $p = 0.10$) (Supplementary Figures 2B and 2C). Results remained largely unaltered after adjusting for WMH volume (NAWM: $b = -0.002$ SUVR/y, $p = 0.02$; WMH: $b = -0.003$, $p < 0.001$).

Females show reduced FTP retention in the WM compared to males

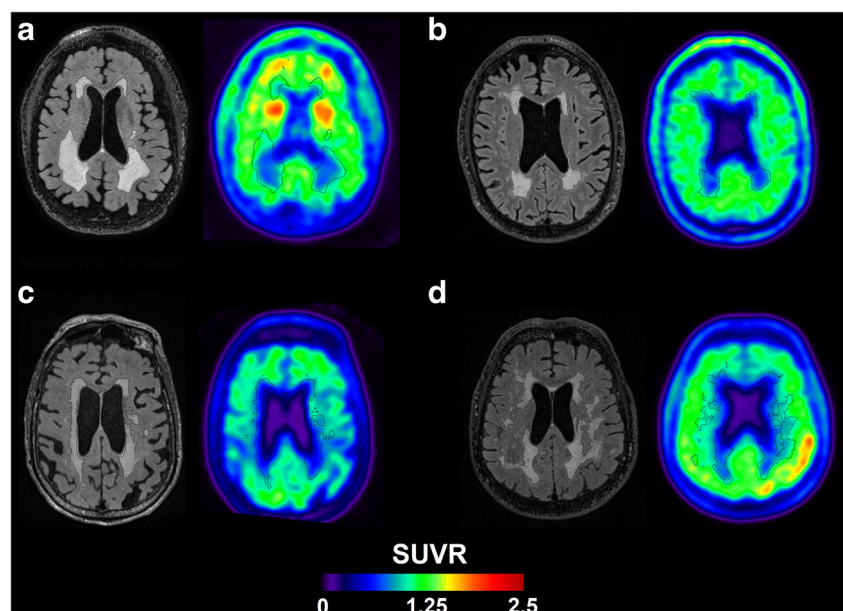
We now tested cross-sectional group-level differences in WM FTP SUVR between females and males. Voxelwise analyses revealed reduced FTP SUVR in female's frontal WM compared to that of males, as well as reduced FTP SUVR in

bilateral WM regions adjacent to the putamen and thalamus (Fig. 4). Reduced FTP SUVR in the WM of females was also found for NAWM (-0.034 SUVR, $p = 0.002$) and WMH (-0.030 , $p = 0.008$) regions.

FTP retention in the WM decreases over time

Linear mixed effects models on longitudinal data at the voxel level demonstrated that FTP retention in the WM decreased over time, involving extensive WM areas that resembled the cross-sectional spatial pattern observed with advancing age (Fig. 5A). Association maps in the WM remained largely unchanged when applying PVE correction (Supplementary Figure 4A). Consistent findings were observed in longitudinal ROI-level analyses: WM FTP SUVRs significantly decreased over time for both NAWM and WMH, although this decrease appeared to be more pronounced for WMH (Fig. 5B and 5C). These results were still significant after performing PVE correction (Supplementary Figures 4B and 4C). Furthermore, longitudinal FTP SUVR decreases were also observed in cerebellar WM (-0.004 SUVR/y, $p = 0.036$), suggesting that the longitudinal changes observed in NAWM were not driven by the presence or progression of adjacent WMH. This was further confirmed by observing that, after adjustment for WMH volume change, voxelwise association patterns remained largely unchanged (Supplementary Figure 5). In line with these findings, ROI-level analyses demonstrated that the time \times WMH change interaction term was not statistically significant for NAWM ($b = -0.0025$ SUVR/cm³, $p = 0.22$), while both interaction and time terms were statistically significant for WMH ($b_{\text{interaction}} = -0.005$ SUVR/cm³, $p = 0.02$; $b_{\text{time}} = -0.016$ SUVR/year, $p < 0.001$), suggesting no influence of longitudinal WMH progression on longitudinal FTP

Fig. 2 Representative FLAIR MRI and [¹⁸F]flortaucipir PET images of four study participants showing reduced [¹⁸F]flortaucipir retention in WMH compared to NAWM. (A) Eighty-year-old participant with MCI, NAWM SUVR = 1.27, WMH SUVR = 1.03; (B) 83-year-old participant with MCI, NAWM SUVR = 1.12, WMH SUVR = 0.88; (C) 87-year-old participant with AD dementia, NAWM SUVR = 0.94, WMH SUVR = 0.74; (D) 82-year-old participant with AD dementia, NAWM SUVR = 1.06, WMH SUVR = 0.85. NAWM, normal-appearing white matter (eroded); WMH, white matter hyperintensity (eroded); SUVR, standardized uptake value ratio; A β , amyloid- β



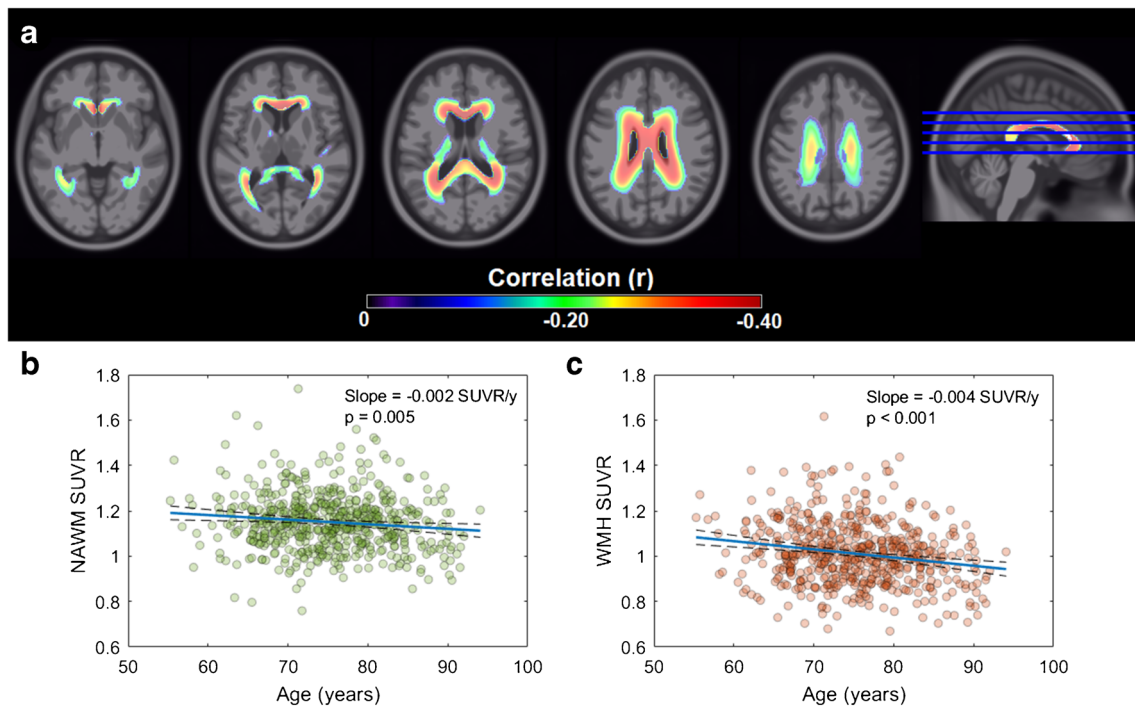


Fig. 3 (A) Voxelwise analysis assessing the cross-sectional negative correlation between [^{18}F]flortaucipir SUVR in WM and age. Statistical maps were thresholded using a voxel-level $p_{\text{FDR}} < 0.001$ threshold and a cluster-level $p_{\text{FWE}} < 0.001$ threshold. (B) Association between [^{18}F]flortaucipir SUVR in NAWM and age. (C) Association between

[^{18}F]flortaucipir SUVR in WMH and age. These results remained largely unchanged when applying two-compartment PVE correction (Supplementary Figure 2). SUVR, standardized uptake value ratio; WM, white matter; NAWM, normal-appearing white matter (eroded); WMH, white matter hyperintensity (eroded)

SUVR in the WM. These results held up after applying two-compartment PVE correction (NAWM: $b_{\text{int}} = -0.001$ SUVR/cm 3 , $p = 0.65$; WMH: $b_{\text{int}} = -0.0002$ SUVR/cm 3 , $p = 0.94$). When fitting linear mixed models with a sex \times time interaction term, no statistically significant sex differences in longitudinal FTP SUVR in the WM were found, both in voxelwise analyses (at $p_{\text{FDR}} < 0.05$) and in NAWM (0.01 SUVR/year, $p = 0.08$, males as reference) and WMH (0.01 SUVR/year, $p = 0.15$) regions.

FTP retention changes in the WM influence cortical FTP retention changes when using WM reference regions

Cross-sectionally, higher WMH volumes were associated with lower FTP SUVR (using inferior cerebellar grey

matter as the reference region) in both the ADNI and the PERSI WM reference regions ($b_{\text{ADNI}} = -0.0012$ SUVR/cm 3 , $p = 0.01$ and $b_{\text{PERSI}} = -0.0008$ SUVR/cm 3 , $p = 0.048$). Regressing annual changes in the temporal cortical Meta-ROI SUVR (using eroded WM as the reference region) on the ADNI WM reference region SUVR changes (using inferior cerebellar grey as the reference region), we observed that 57% of the variance in increases of cortical SUVR was explained by longitudinal decreases in the ADNI WM reference region (Fig. 6A). When stratifying by cognitive status, variance in longitudinal changes in the Meta-ROI SUVR was also strongly explained by changes in the ADNI WM SUVR in both CU and CI individuals (43% for CU and 66% for CI, respectively, Fig. 6B). Restricting analyses to A β + subjects yielded similar findings (Fig. 6C). Compared to the ADNI WM reference

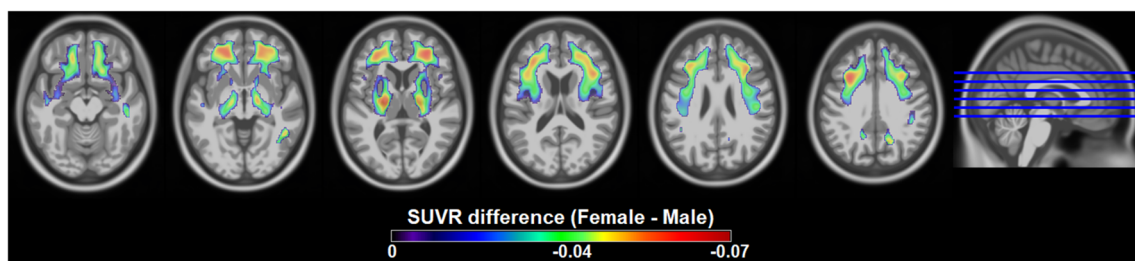


Fig. 4 Exploratory voxelwise analysis assessing cross-sectional mean [^{18}F]flortaucipir SUVR differences between females and males, adjusted for age. Statistical maps in this exploratory analysis were thresholded using a more lenient threshold of $p_{\text{FDR}} < 0.05$

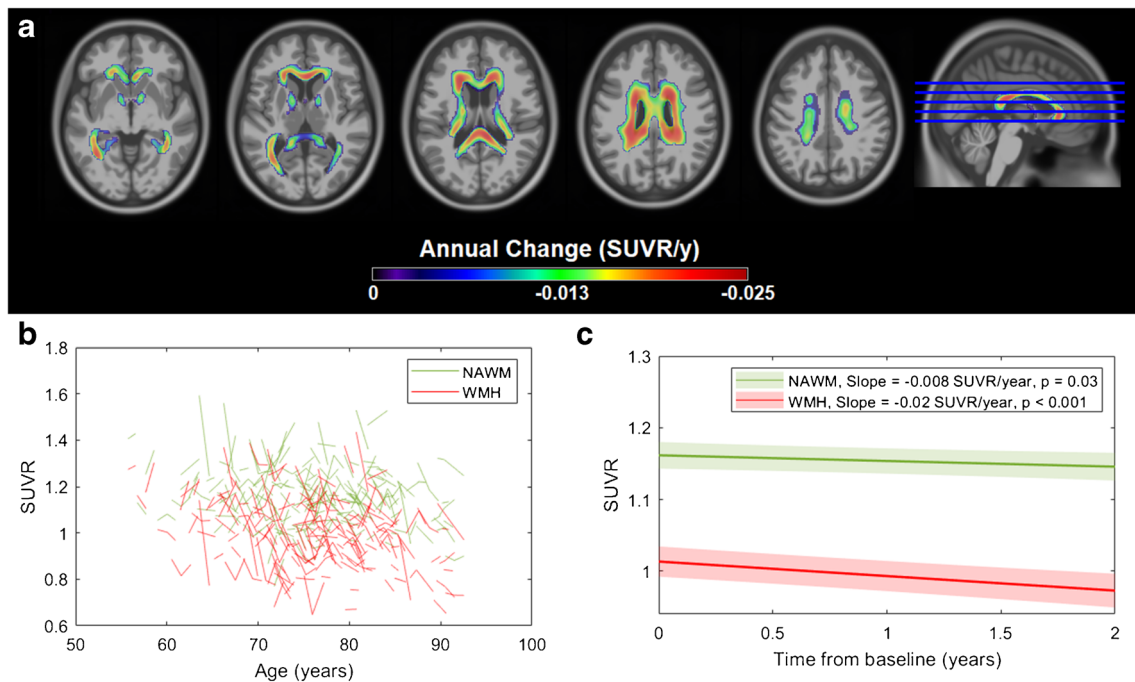


Fig. 5 (A) Voxelwise analysis assessing WM areas in which [^{18}F]flortaucipir SUVR significantly decreased over time. Statistical maps were thresholded using a voxel-level $p_{\text{FDR}} < 0.001$ threshold and a cluster-level $p_{\text{FWE}} < 0.001$ threshold. (B) Spaghetti plot showing the [^{18}F]flortaucipir SUVR trajectories in NAWM and WMH as a function of age. (C) Average longitudinal trajectories for NAWM and WMH

[^{18}F]flortaucipir SUVR as estimated by linear mixed model analysis. These results remained statistically significant after applying two-compartment PVE correction (Supplementary Figure 4). SUVR, standardized uptake value ratio; WM, white matter; NAWM, normal-appearing white matter (eroded); WMH, white matter hyperintensity (eroded)

region, SUVR changes in the PERSI WM reference were less strongly associated with changes in the PERSI-referenced cortical Meta-ROI SUVR, although these variations still explained a significant fraction of the observed variance (from 17% in $\text{A}\beta + \text{CI}$ to 36% in $\text{A}\beta + \text{CU}$).

Discussion

In this study, we investigated how WM lesions, assessed as WMH, and age influence FTP retention in the WM. Furthermore, we estimated how FTP retention in the WM changes over time and investigated how these longitudinal changes influenced longitudinal cortical FTP SUVRs when using a WM reference region. Our findings indicate that (1) FTP retention in WMH is lower than in NAWM, (2) advancing age is associated with lower FTP retention in WM, (3) FTP retention in the WM decreases over time, and (4) a significant fraction of the variance observed in longitudinal changes of WM-referenced cortical FTP measures can be attributed to WM signal decreases. Overall, these results reveal non-trivial pathologic and dynamic correlates of FTP retention in the WM and highlight potentially important shortcomings of using WM reference regions for longitudinal FTP PET imaging.

Although FTP retention in the WM is poorly understood, the affinity of tau tracers for β -sheet structures [23] led us to hypothesize that FTP retention in WM could partially be explained by FTP binding to the β -sheet structure exhibited by the myelin basic protein. Such a myelin mechanism was previously proposed to explain the high WM signal characteristic for $\text{A}\beta$ tracers [21], which also display affinity for β -sheet structures, and this mechanism was subsequently supported by several studies using $\text{A}\beta$ PET to assess demyelination in multiple sclerosis and animal models [21, 22, 24–26, 47]. Here, our findings of lower FTP retention in the WM associated to WMH and advancing age, as well as longitudinal decreases over time, are supportive of a similar myelin mechanism for explaining FTP binding in the WM: WMH areas typically reflect severe demyelination [31, 48] and generalized myelin loss occurs with aging [49, 50]. Interestingly, we also found that females showed reduced cross-sectional FTP retention in specific WM regions. Although the association pattern adjacent to the thalamus and putamen is likely driven by PVE [51], we did find prominent decreases in bilateral WM regions of the frontal lobe that cannot be explained by these effects. Though establishing the precise underlying mechanism lies beyond the scope of this study, we hypothesize that this result could be driven by menopause-related demyelination, as proposed by several previous reports [33, 34]. This hypothesis is further supported by the regionality of our

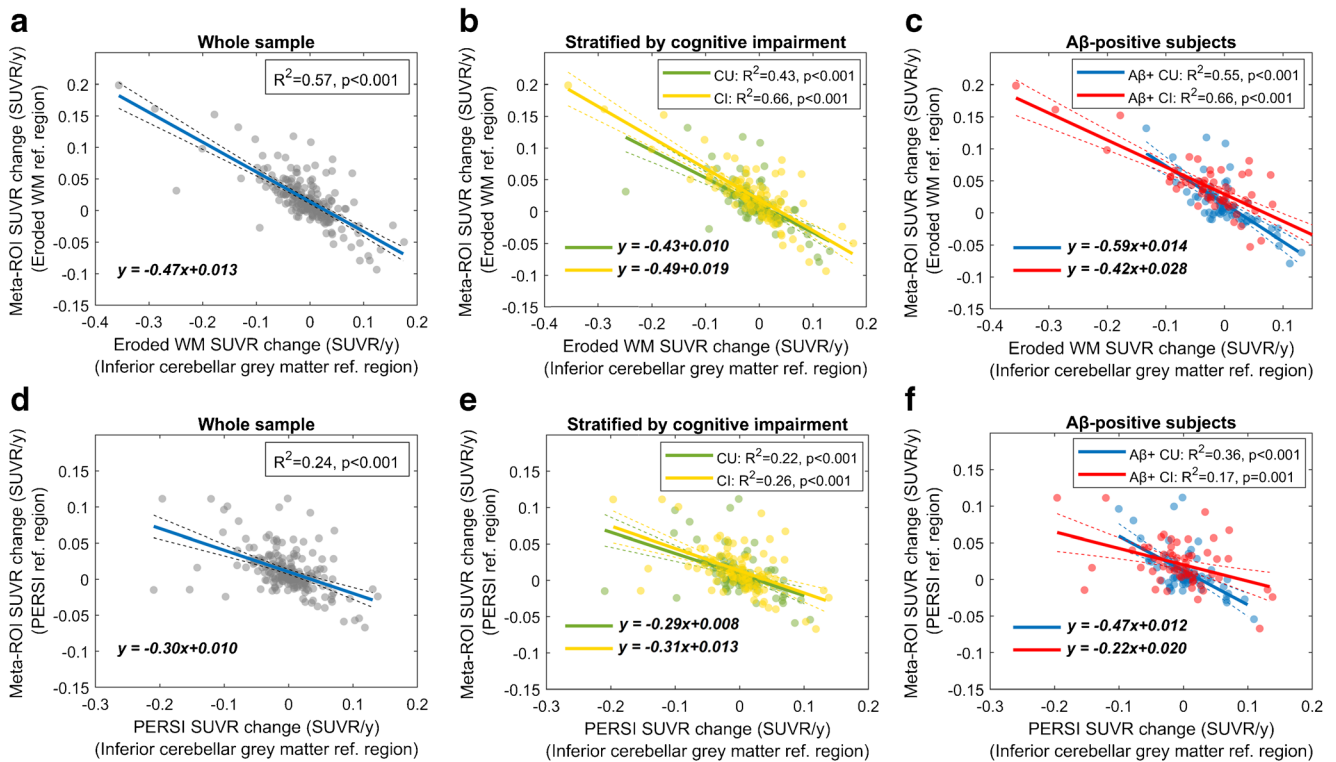


Fig. 6 Correlations of [18 F]flortaucipir SUVR annual change (computed using the inferior cerebellar cortex as the reference region) in the ADNI (A–C) and the PERSI (D–F) WM reference regions with [18 F]flortaucipir SUVR annual change (computed using the ADNI or the PERSI WM reference regions) in the AD cortical Meta-ROI. Analyses were

presented for the whole sample (A and D), stratified by cognitive impairment (B and E), and stratified by cognitive impairment in Aβ+ individuals (C and F). Linear regression equations were reported in the same units as those used in the plots. SUVR, standardized uptake value ratio; WM, white matter; AD, Alzheimer’s disease; Aβ, amyloid-β

findings, as menopausal hormone therapy has been found to be specifically associated with lower rates of atrophy in the frontal lobe [52, 53]. Overall, these results contribute to a better understanding of the pathologic and dynamic correlates of FTP retention in the WM and further suggests a potential utility of FTP imaging in demyelinating diseases, although at this point further dedicated studies are needed to systematically investigate this scenario.

The findings of this study have clear implications for the use of WM reference regions in longitudinal FTP PET imaging. Ideally, an effective reference region for longitudinal PET imaging should not show any specific binding and a relatively stable reference-to-target non-specific binding ratio over the study duration [54]. According to our study results, this does not seem to be the case for WM reference regions in FTP imaging: WMH, which are common in both normal aging [48, 55] and AD [56, 57], significantly influenced FTP retention. Among elderly subjects, significant longitudinal increases in WMH burden over typical time frames for clinical trials (1–2 years) have been demonstrated [58]. Given the significantly lower FTP retention in WMH areas, these increases in WMH burden might be erroneously interpreted as increases in cortical tau load if WM reference regions are used for calculation of cortical FTP SUVR. Similarly, recent evidence now indicates links between WMH and Aβ pathology

[39, 46, 59], highlighting the confounding potential of WMH in AD. Interestingly, we also observed age-related and longitudinal FTP retention decreases in NAWM, suggesting that other mechanisms such as age-related myelin loss could play a non-negligible role in explaining FTP retention in WM. In longitudinal regression analyses, we estimated that between 44% and 66% of the variance observed in cortical FTP SUVR increases were explained by longitudinal signal decreases in the ADNI WM reference region. Similarly, but less pronounced, longitudinal FTP SUVR changes in the PERSI reference region accounted for 17% to 36% of the observed variance. The strength of these correlations suggests that even small FTP retention changes in the WM reference region might have a very relevant impact in longitudinal WM-referenced cortical FTP measurements. Together, these results highlight potential shortcomings in the use of WM reference regions for longitudinal FTP imaging that may reduce clinical trial efficiency and increase costs.

Though studying the impact of WM pathology on the derivation of the PERSI reference region lies beyond the scope of this study, we believe that our results have interesting implications for the aforementioned method. The PERSI method assumes that the WM signal can be decomposed in two Gaussian components, one describing spill-in counts from the WM and the second describing “pure” WM signal [20]. However, the approach is

agnostic to the fact that a significant fraction of WM voxels can show reduced FTP retention due to WM pathology, and thus the distribution of WM intensities might no longer be accurately modeled with two Gaussian components. As a result, the PERSI reference region might include either a significant fraction of voxels affected by spill-in counts or influenced by WM pathology, potentially reducing the benefits of the method. On the other hand, in subjects with low cortical signal, PERSI might result in unexpected benefits. Since these subjects do not show the “spill-in” peak, the second peak of the PERSI method will describe the low-intensity distribution associated to WM pathology and therefore the method will automatically remove these particularly problematic voxels. These findings expose the need for future dedicated studies evaluating in detail the impact of WM pathology in the derivation of data-driven WM reference regions.

WMH are usually distributed along periventricular areas [57], and therefore FTP SUVRs in WMHs might be affected by PVE with low intensity CSF signal. To avoid this problem, we performed a 3-mm erosion procedure, which was also used in a previous study with an A β PET tracer [29], which found an average difference of 0.14 SUVR units between NAWM and WMH. This difference is unlikely to be driven by potential residual PVE due to WMH spill-out to CSF since our findings remained unchanged after correcting for these PVE. It is also unlikely that the observed difference is driven by potential residual spill-in counts in NAWM coming from high-intensity cortical GM signal of subjects with elevated tau burden since this difference was also observed among A β - subjects (Fig. 1B), in which elevated cortical tau burden is very rare [60]. Recent FTP studies demonstrated that the basal ganglia show significant age-related off-target binding [51, 61], which might have influenced our observation of age-dependent FTP retention in WM. However, this off-target binding increased with age [61] and therefore cannot explain our observed age-related decrease in FTP retention in the WM. Together, these observations strongly suggest that our findings reflect biological effects rather than technical limitations of FTP PET imaging.

The present study has several strengths and limitations. We analyzed a large and well-characterized cohort of elderly subjects spanning the entire AD continuum with multimodal PET and MRI scans. This cohort can be considered a good proxy of a clinical trial cohort and therefore our findings might have direct implications for clinical trials using FTP PET as outcome measure. Another strength is the longitudinal design of the study, which allowed us to confirm some of the observed cross-sectional associations. A limitation of our study is that the ADNI is a highly preselected cohort that only includes subjects with relatively low vascular pathology. Given the direct links between WM pathology and FTP retention, it is unclear whether the size of the effects observed in this study would remain similar among subjects with higher vascular burden.

In conclusion, we have demonstrated that WM pathology and advancing age influence FTP retention in the WM, and further showed that this retention changes over a mean follow-up of 1.5 years. These findings are consistent with the hypothesis that FTP signal in the WM could be at least partially due to binding to the myelin basic protein, highlighting the potential of FTP imaging in demyelinating diseases. Dynamic changes of FTP retention in the WM, which are exacerbated by common age-related WM pathologies such as WMH, argue against the use of WM reference regions for longitudinal FTP PET imaging. Future studies are warranted to explore whether second-generation tau tracers show similar WM retention properties.

Supplementary Information The online version contains supplementary material available at <https://doi.org/10.1007/s00259-021-05195-5>.

Acknowledgments Data collection and sharing for this project was funded by the Alzheimer’s Disease Neuroimaging Initiative (ADNI) (National Institutes of Health Grant U01 AG024904) and DOD ADNI (Department of Defense award number W81XWH-12-2-0012). ADNI is funded by the National Institute on Aging, the National Institute of Biomedical Imaging and Bioengineering, and through generous contributions from the following: AbbVie, Alzheimer’s Association; Alzheimer’s Drug Discovery Foundation; Araclon Biotech; BioClinica, Inc.; Biogen; Bristol-Myers Squibb Company; CereSpir, Inc.; Cogstate; Eisai Inc.; Elan Pharmaceuticals, Inc.; Eli Lilly and Company; EuroImmun; F. Hoffmann-La Roche Ltd and its affiliated company Genentech, Inc.; Fujirebio; GE Healthcare; IXICO Ltd.; Janssen Alzheimer Immunotherapy Research & Development, LLC.; Johnson & Johnson Pharmaceutical Research & Development LLC.; Lumosity; Lundbeck; Merck & Co., Inc.; Meso Scale Diagnostics, LLC.; NeuroRx Research; Neurotrack Technologies; Novartis Pharmaceuticals Corporation; Pfizer Inc.; Piramal Imaging; Servier; Takeda Pharmaceutical Company; and Transition Therapeutics. The Canadian Institutes of Health Research is providing funds to support ADNI clinical sites in Canada. Private sector contributions are facilitated by the Foundation for the National Institutes of Health (www.fnih.org). The grantee organization is the Northern California Institute for Research and Education, and the study is coordinated by the Alzheimer’s Therapeutic Research Institute at the University of Southern California. ADNI data are disseminated by the Laboratory for Neuro Imaging at the University of Southern California.

Funding MJG is supported by the “Miguel Servet” program (CP19/00031) of the Spanish Instituto de Salud Carlos III (ISCIII-FEDER). MS is supported by the Knut and Alice Wallenberg Foundation (Wallenberg Centre for Molecular and Translational Medicine; KAW 2014.0363), the Swedish Research Council (#2017-02869), the Swedish state under the agreement between the Swedish government and the County Councils, the ALF-agreement (#ALFGBG-813971), and the Swedish Alzheimer Foundation (#AF-740191).

Data availability All the data used in this study is publicly available at the Laboratory of Neuro Imaging (LONI) server of the Alzheimer’s Disease Neuroimaging Initiative.

Compliance with ethical standards

Conflict of interest The authors declare that they have no conflict of interest.

Ethics approval All participants provided written informed consent approved by the institutional review board of each ADNI participating institution.

Code availability Custom code used in this study will be shared to interested investigators upon request.

References

- Fleisher AS, Pontecorvo MJ, Devous MD Sr, Lu M, Arora AK, Trucchio SP, et al. Positron emission tomography imaging with [18F]flortaucipir and postmortem assessment of Alzheimer disease neuropathologic changes. *JAMA Neurol.* 2020. <https://doi.org/10.1001/jamaneurol.2020.0528>.
- Lowe VJ, Lundt ES, Albertson SM, Min HK, Fang P, Przybelski SA, et al. Tau-positron emission tomography correlates with neuropathology findings. *Alzheimers Dement.* 2020;16:561–71. <https://doi.org/10.1016/j.jalz.2019.09.079>.
- Smith R, Wibom M, Pawlik D, Englund E, Hansson O. Correlation of in vivo [18F]Flortaucipir with postmortem Alzheimer disease tau pathology. *JAMA Neurol.* 2019;76:310–7. <https://doi.org/10.1001/jamaneurol.2018.3692>.
- Hyman BT, Phelps CH, Beach TG, Bigio EH, Cairns NJ, Carrillo MC, et al. National Institute on Aging-Alzheimer's Association guidelines for the neuropathologic assessment of Alzheimer's disease. *Alzheimers Dement.* 2012;8:1–13. <https://doi.org/10.1016/j.jalz.2011.10.007>.
- Nelson PT, Alafuzoff I, Bigio EH, Bouras C, Braak H, Cairns NJ, et al. Correlation of Alzheimer disease neuropathologic changes with cognitive status: a review of the literature. *J Neuropathol Exp Neurol.* 2012;71:362–81. <https://doi.org/10.1097/NEN.0b013e31825018f7>.
- Hanseeuw BJ, Betensky RA, Jacobs HIL, Schultz AP, Sepulcre J, Becker JA, et al. Association of amyloid and tau with cognition in preclinical Alzheimer disease: a longitudinal study. *JAMA Neurol.* 2019. <https://doi.org/10.1001/jamaneurol.2019.1424>.
- La Joie R, Visani AV, Baker SL, Brown JA, Bourakova V, Cha J, et al. Prospective longitudinal atrophy in Alzheimer's disease correlates with the intensity and topography of baseline tau-PET. *Sci Transl Med.* 2020;12. <https://doi.org/10.1126/scitranslmed.aau5732>.
- Aschenbrenner AJ, Gordon BA, Benzinger TLS, Morris JC, Hassenstab JJ. Influence of tau PET, amyloid PET, and hippocampal volume on cognition in Alzheimer disease. *Neurology.* 2018;91:e859–e66. <https://doi.org/10.1212/WNL.0000000000006075>.
- Pontecorvo MJ, Devous MD Sr, Navitsky M, Lu M, Salloway S, Schaerff FW, et al. Relationships between flortaucipir PET tau binding and amyloid burden, clinical diagnosis, age and cognition. *Brain.* 2017;140:748–63. <https://doi.org/10.1093/brain/aww334>.
- Brier MR, Gordon B, Friedrichsen K, McCarthy J, Stern A, Christensen J, et al. Tau and abeta imaging, CSF measures, and cognition in Alzheimer's disease. *Sci Transl Med.* 2016;8:338ra66. <https://doi.org/10.1126/scitranslmed.aaf2362>.
- Ossenkoppele R, Smith R, Ohlsson T, Strandberg O, Mattsson N, Insel PS, et al. Associations between tau, Abeta, and cortical thickness with cognition in Alzheimer disease. *Neurology.* 2019;92:e601–e12. <https://doi.org/10.1212/WNL.0000000000006875>.
- Lowe VJ, Bruinsma TJ, Wiste HJ, Min HK, Weigand SD, Fang P, et al. Cross-sectional associations of tau-PET signal with cognition in cognitively unimpaired adults. *Neurology.* 2019;93:e29–39. <https://doi.org/10.1212/WNL.0000000000007728>.
- Gauthier S, Albert M, Fox N, Goedert M, Kivipelto M, Mestre-Ferrandiz J, et al. Why has therapy development for dementia failed in the last two decades? *Alzheimers Dement.* 2016;12:60–4. <https://doi.org/10.1016/j.jalz.2015.12.003>.
- Congdon EE, Sigurdsson EM. Tau-targeting therapies for Alzheimer disease. *Nat Rev Neurol.* 2018;14:399–415. <https://doi.org/10.1038/s41582-018-0013-z>.
- Jack CR Jr, Wiste HJ, Schwarz CG, Lowe VJ, Senjem ML, Vemuri P, et al. Longitudinal tau PET in ageing and Alzheimer's disease. *Brain.* 2018;141:1517–28. <https://doi.org/10.1093/brain/awy059>.
- Pontecorvo MJ, Devous MD, Kennedy I, Navitsky M, Lu M, Galante N, et al. A multicentre longitudinal study of flortaucipir (18F) in normal ageing, mild cognitive impairment and Alzheimer's disease dementia. *Brain.* 2019;142:1723–35. <https://doi.org/10.1093/brain/awz090>.
- Baek MS, Cho H, Lee HS, Choi JY, Lee JH, Ryu YH, et al. Temporal trajectories of in vivo tau and amyloid-beta accumulation in Alzheimer's disease. *Eur J Nucl Med Mol Imaging.* 2020. <https://doi.org/10.1007/s00259-020-04773-3>.
- Hansson O, Mormino EC. Is longitudinal tau PET ready for use in Alzheimer's disease clinical trials? *Brain.* 2018;141:1241–4. <https://doi.org/10.1093/brain/awy065>.
- Harrison TM, La Joie R, Maass A, Baker SL, Swinnerton K, Fenton L, et al. Longitudinal tau accumulation and atrophy in aging and Alzheimer disease. *Ann Neurol.* 2019;85:229–40. <https://doi.org/10.1002/ana.25406>.
- Southeikal S, Devous MD Sr, Kennedy I, Navitsky M, Lu M, Joshi AD, et al. Flortaucipir F 18 quantitation using parametric estimation of reference signal intensity. *J Nucl Med.* 2018;59:944–51. <https://doi.org/10.2967/jnumed.117.200006>.
- Stankoff B, Freeman L, Aigrot MS, Chardain A, Dolle F, Williams A, et al. Imaging central nervous system myelin by positron emission tomography in multiple sclerosis using [methyl-(1)(1)C]-2-(4'-methylaminophenyl)-6-hydroxybenzothiazole. *Ann Neurol.* 2011;69:673–80. <https://doi.org/10.1002/ana.22320>.
- Faria Dde P, Copray S, Sijbesma JW, Willemsen AT, Buchpiguel CA, Dierckx RA, et al. PET imaging of focal demyelination and remyelination in a rat model of multiple sclerosis: comparison of [11C]MeDAS, [11C]CIC and [11C]PIB. *Eur J Nucl Med Mol Imaging.* 2014;41:995–1003. <https://doi.org/10.1007/s00259-013-2682-6>.
- Leuzy A, Chiotis K, Lemoine L, Gillberg PG, Almkvist O, Rodriguez-Vieitez E, et al. Tau PET imaging in neurodegenerative tauopathies—still a challenge. *Mol Psychiatry.* 2019;24:1112–34. <https://doi.org/10.1038/s41380-018-0342-8>.
- Pietroboni AM, Carandini T, Colombi A, Mercurio M, Ghezzi L, Giulietti G, et al. Amyloid PET as a marker of normal-appearing white matter early damage in multiple sclerosis: correlation with CSF beta-amyloid levels and brain volumes. *Eur J Nucl Med Mol Imaging.* 2019;46:280–7. <https://doi.org/10.1007/s00259-018-4182-1>.
- Bodini B, Veronese M, Garcia-Lorenzo D, Battaglini M, Poirion E, Chardain A, et al. Dynamic imaging of individual remyelination profiles in multiple sclerosis. *Ann Neurol.* 2016;79:726–38. <https://doi.org/10.1002/ana.24620>.
- Matias-Guiu JA, Cabrera-Martin MN, Matias-Guiu J, Oreja-Guevara C, Riola-Parada C, Moreno-Ramos T, et al. Amyloid PET imaging in multiple sclerosis: an (18)F-florbetaben study. *BMC Neurol.* 2015;15:243. <https://doi.org/10.1186/s12883-015-0502-2>.
- Zeydan B, Lowe VJ, Schwarz CG, Przybelski SA, Tosakulwong N, Zuk SM, et al. Pittsburgh compound-B PET white matter imaging and cognitive function in late multiple sclerosis. *Mult Scler.* 2018;24:739–49. <https://doi.org/10.1177/1352458517707346>.
- Glodzik L, Rusinek H, Li J, Zhou C, Tsui W, Mosconi L, et al. Reduced retention of Pittsburgh compound B in white matter

- lesions. *Eur J Nucl Med Mol Imaging*. 2015;42:97–102. <https://doi.org/10.1007/s00259-014-2897-1>.
29. Zeydan B, Schwarz CG, Lowe VJ, Reid RI, Przybelski SA, Lesnick TG, et al. Investigation of white matter PiB uptake as a marker of white matter integrity. *Ann Clin Transl Neurol*. 2019;6:678–88. <https://doi.org/10.1002/acn3.741>.
 30. Goodheart AE, Tamburo E, Minhas D, Aizenstein HJ, McDade E, Snitz BE, et al. Reduced binding of Pittsburgh Compound-B in areas of white matter hyperintensities. *Neuroimage Clin*. 2015;9:479–83. <https://doi.org/10.1016/j.nicl.2015.09.009>.
 31. Simpson JE, Fernando MS, Clark L, Ince PG, Matthews F, Forster G, et al. White matter lesions in an unselected cohort of the elderly: astrocytic, microglial and oligodendrocyte precursor cell responses. *Neuropathol Appl Neurobiol*. 2007;33:410–9. <https://doi.org/10.1111/j.1365-2990.2007.00828.x>.
 32. Tang Y, Nyengaard JR, Pakkenberg B, Gundersen HJ. Age-induced white matter changes in the human brain: a stereological investigation. *Neurobiol Aging*. 1997;18:609–15. [https://doi.org/10.1016/s0197-4580\(97\)00155-3](https://doi.org/10.1016/s0197-4580(97)00155-3).
 33. Klosinski LP, Yao J, Yin F, Fonteh AN, Harrington MG, Christensen TA, et al. White matter lipids as a ketogenic fuel supply in aging female brain: implications for Alzheimer's disease. *EBioMedicine*. 2015;2:1888–904. <https://doi.org/10.1016/j.ebiom.2015.11.002>.
 34. He Q, Luo Y, Lv F, Xiao Q, Chao F, Qiu X, et al. Effects of estrogen replacement therapy on the myelin sheath ultrastructure of myelinated fibers in the white matter of middle-aged ovariectomized rats. *J Comp Neurol*. 2018;526:790–802. <https://doi.org/10.1002/cne.24366>.
 35. Landau SM, Breault C, Joshi AD, Pontecorvo M, Mathis CA, Jagust WJ, et al. Amyloid-beta imaging with Pittsburgh compound B and florbetapir: comparing radiotracers and quantification methods. *J Nucl Med*. 2013;54:70–7. <https://doi.org/10.2967/jnumed.112.109009>.
 36. Jagust WJ, Landau SM, Koeppe RA, Reiman EM, Chen K, Mathis CA, et al. The Alzheimer's Disease Neuroimaging Initiative 2 PET Core: 2015. *Alzheimers Dement*. 2015;11:757–71. <https://doi.org/10.1016/j.jalz.2015.05.001>.
 37. Jack CR Jr, Barnes J, Bernstein MA, Borowski BJ, Brewer J, Clegg S, et al. Magnetic resonance imaging in Alzheimer's Disease Neuroimaging Initiative 2. *Alzheimers Dement*. 2015;11:740–56. <https://doi.org/10.1016/j.jalz.2015.05.002>.
 38. Schmidt P, Gaser C, Arsic M, Buck D, Forschler A, Berthele A, et al. An automated tool for detection of FLAIR-hyperintense white-matter lesions in multiple sclerosis. *Neuroimage*. 2012;59:3774–83. <https://doi.org/10.1016/j.neuroimage.2011.11.032>.
 39. Moscoso A, Rey-Bretal D, Silva-Rodriguez J, Aldrey JM, Cortes J, Pias-Peleiteiro J, et al. White matter hyperintensities are associated with subthreshold amyloid accumulation. *Neuroimage*. 2020;218:116944. <https://doi.org/10.1016/j.neuroimage.2020.116944>.
 40. Sudre CH, Cardoso MJ, Ourselin S. Alzheimer's Disease Neuroimaging I. Longitudinal segmentation of age-related white matter hyperintensities. *Med Image Anal*. 2017;38:50–64. <https://doi.org/10.1016/j.media.2017.02.007>.
 41. Maass A, Landau S, Baker SL, Horng A, Lockhart SN, La Joie R, et al. Comparison of multiple tau-PET measures as biomarkers in aging and Alzheimer's disease. *Neuroimage*. 2017;157:448–63. <https://doi.org/10.1016/j.neuroimage.2017.05.058>.
 42. Baker SL, Maass A, Jagust WJ. Considerations and code for partial volume correcting [(18)F]-AV-1451 tau PET data. *Data Brief*. 2017;15:648–57. <https://doi.org/10.1016/j.dib.2017.10.024>.
 43. Meltzer CC, Leal JP, Mayberg HS, Wagner HN Jr, Frost JJ. Correction of PET data for partial volume effects in human cerebral cortex by MR imaging. *J Comput Assist Tomogr*. 1990;14:561–70. <https://doi.org/10.1097/00004728-199007000-00011>.
 44. Jack CR Jr, Wiste HJ, Weigand SD, Therneau TM, Lowe VJ, Knopman DS, et al. Defining imaging biomarker cut points for brain aging and Alzheimer's disease. *Alzheimers Dement*. 2017;13:205–16. <https://doi.org/10.1016/j.jalz.2016.08.005>.
 45. Landau SM, Fero A, Baker SL, Koeppe R, Mintun M, Chen K, et al. Measurement of longitudinal beta-amyloid change with 18F-florbetapir PET and standardized uptake value ratios. *J Nucl Med*. 2015;56:567–74. <https://doi.org/10.2967/jnumed.114.148981>.
 46. Graff-Radford J, Arenaza-Urquijo EM, Knopman DS, Schwarz CG, Brown RD, Rabinstein AA, et al. White matter hyperintensities: relationship to amyloid and tau burden. *Brain*. 2019;142:2483–91. <https://doi.org/10.1093/brain/awz162>.
 47. Pytel V, Matias-Guiu JA, Matias-Guiu J, Cortes-Martinez A, Montero P, Moreno-Ramos T, et al. Amyloid PET findings in multiple sclerosis are associated with cognitive decline at 18 months. *Mult Scler Relat Disord*. 2020;39:101926. <https://doi.org/10.1016/j.msard.2020.101926>.
 48. Murray ME, Vemuri P, Preboske GM, Murphy MC, Schweitzer KJ, Parisi JE, et al. A quantitative postmortem MRI design sensitive to white matter hyperintensity differences and their relationship with underlying pathology. *J Neuropathol Exp Neurol*. 2012;71:1113–22. <https://doi.org/10.1097/NEN.0b013e318277387e>.
 49. Hasan KM, Kamali A, Abid H, Kramer LA, Fletcher JM, Ewing-Cobbs L. Quantification of the spatiotemporal microstructural organization of the human brain association, projection and commissural pathways across the lifespan using diffusion tensor tractography. *Brain Struct Funct*. 2010;214:361–73. <https://doi.org/10.1007/s00429-009-0238-0>.
 50. Westlye LT, Walhovd KB, Dale AM, Bjornerud A, Due-Tonnessen P, Engvig A, et al. Life-span changes of the human brain white matter: diffusion tensor imaging (DTI) and volumetry. *Cereb Cortex*. 2010;20:2055–68. <https://doi.org/10.1093/cercor/bhp280>.
 51. Baker SL, Harrison TM, Maass A, La Joie R, Jagust WJ. Effect of off-target binding on (18)F-Flortaucipir variability in healthy controls across the life span. *J Nucl Med*. 2019;60:1444–51. <https://doi.org/10.2967/jnumed.118.224113>.
 52. Kantarci K, Tosakulwong N, Lesnick TG, Zuk SM, Lowe VJ, Fields JA, et al. Brain structure and cognition 3 years after the end of an early menopausal hormone therapy trial. *Neurology*. 2018;90:e1404–e12. <https://doi.org/10.1212/WNL.0000000000005325>.
 53. Boyle CP, Raji CA, Erickson KI, Lopez OL, Becker JT, Gach HM, et al. Estrogen, brain structure, and cognition in postmenopausal women. *Hum Brain Mapp*. 2020. <https://doi.org/10.1002/hbm.25200>.
 54. Lopez-Gonzalez FJ, Moscoso A, Efthimiou N, Fernandez-Ferreiro A, Pineiro-Fiel M, Archibald SJ, et al. Spill-in counts in the quantification of (18)F-florbetapir on Abeta-negative subjects: the effect of including white matter in the reference region. *EJNMMI Phys*. 2019;6:27. <https://doi.org/10.1186/s40658-019-0258-7>.
 55. Habes M, Erus G, Toledo JB, Zhang T, Bryan N, Launer LJ, et al. White matter hyperintensities and imaging patterns of brain ageing in the general population. *Brain*. 2016;139:1164–79. <https://doi.org/10.1093/brain/aww008>.
 56. Gouw AA, Seewann A, Vrenken H, van der Flier WM, Rozemuller JM, Barkhof F, et al. Heterogeneity of white matter hyperintensities in Alzheimer's disease: post-mortem quantitative MRI and neuropathology. *Brain*. 2008;131:3286–98. <https://doi.org/10.1093/brain/awn265>.
 57. Gootjes L, Teipel SJ, Zebuhr Y, Schwarz R, Leinsinger G, Scheltens P, et al. Regional distribution of white matter hyperintensities in vascular dementia, Alzheimer's disease and healthy aging. *Dement Geriatr Cogn Disord*. 2004;18:180–8. <https://doi.org/10.1159/000079199>.
 58. Carmichael O, Schwarz C, Drucker D, Fletcher E, Harvey D, Beckett L, et al. Longitudinal changes in white matter disease and

- cognition in the first year of the Alzheimer disease neuroimaging initiative. *Arch Neurol.* 2010;67:1370–8. <https://doi.org/10.1001/archneurol.2010.284>.
59. Caballero MAA, Song Z, Rubinski A, Duering M, Dichgans M, Park DC, et al. Age-dependent amyloid deposition is associated with white matter alterations in cognitively normal adults during the adult life span. *Alzheimers Dement.* 2020;16:651–61. <https://doi.org/10.1002/alz.12062>.
60. Jack CR, Wiste HJ, Botha H, Weigand SD, Therneau TM, Knopman DS, et al. The bivariate distribution of amyloid-beta and tau: relationship with established neurocognitive clinical syndromes. *Brain.* 2019;142:3230–42. <https://doi.org/10.1093/brain/awz268>.
61. Choi JY, Cho H, Ahn SJ, Lee JH, Ryu YH, Lee MS, et al. Off-target (18)F-AV-1451 binding in the basal ganglia correlates with age-related iron accumulation. *J Nucl Med.* 2018;59:117–20. <https://doi.org/10.2967/jnumed.117.195248>.

Publisher's note Springer Nature remains neutral with regard to jurisdictional claims in published maps and institutional affiliations.